doi:10.1016/j.jmb.2005.01.031 J. Mol. Biol. (2005) 347, 309–321

JMB

Available online at www.sciencedirect.com

SCIENCE DIRECT®

ELSEVIER

Structure of the Adaptor Protein p14 Reveals a Profilin-like Fold with Distinct Function

Chengmin Qian, Qiang Zhang, Xueqi Wang, Lei Zeng, Amjad Farooq* and Ming-Ming Zhou*

Structural Biology Program Department of Physiology and Biophysics, Mount Sinai School of Medicine, One Gustave L. Levy Place, New York, NY 10029, USA

The adaptor protein p14 is associated with the cytoplasmic face of late endosomes that is involved in cell-surface receptor endocytosis and it also directly interacts with MP1, a scaffolding protein that binds the MAP kinase ERK1 and its upstream kinase activator MEK1. The interaction of p14 with MP1 recruits the latter to late endosomes and the endosomal localization of p14/MP1-MEK1-ERK1 scaffolding complex is required for signaling *via* ERK MAP kinase in an efficient and specific manner upon receptor stimulation. Here, we report the three-dimensional solution structure of the adaptor protein p14. The structure reveals a profilin-like fold with a central five-stranded β-sheet sandwiched between α-helices. Unlike profilin, however, p14 exhibits weak interaction with selective phosphoinositides but no affinity towards proline-rich sequences. Structural comparison between profilin and p14 reveals the molecular basis for the differences in these functions. We further mapped the MP1 binding sites on p14 by NMR, and discuss the implications of these important findings on the possible function of p14.

*Corresponding authors

Keywords: MAP kinase; MP1; p14; three-dimensional structure; NMR

Introduction

Cell-surface growth factor receptors utilize a number of mechanisms in the transmission of information from the outside to the inside of the cell.[1] Upon the binding of extracellular stimuli such as hormones, growth factors, cytokines and antigens, the activated growth factor receptors can either directly recruit and activate effector enzymes such as phospholipase Cγ and phosphatidylinositol-3′-kinase, or alternatively, they can activate downstream effector enzymes through the recruitment of a plethora of adaptor proteins and protein modules.[2] For example, the activated, tyrosine-phosphorylated epidermal growth factor (EGF) receptor recruits the adaptor protein Shc through specific interaction with its phosphotyrosine binding domain,[3,4] resulting in tyrosine-phosphorylation of Shc. This enables Shc to bind to the *Src* homology 2 domain of Grb2, which in turn interacts with the guanine nucleotide exchange factor SOS.[5,6] The activated SOS causes GDP–GTP exchange within the Ras allowing it in turn to activate the three-tier mitogen-activated protein kinase (MAPK) cascade from Raf to MEK to ERK. Upon activation, MAPKs such as ERK mediate key cellular events in the cytoplasm including phosphorylation of membrane-associated and cytoplasmic proteins such as kinases, cytoskeletal elements, phospholipase A_2 and stathmin.[7] MAPKs may also translocate to the nucleus to phosphorylate specific transcription factors such as c-Jun, c-Fos, Elk-1 and c-Myc.[8]

More recent studies have revealed that the activated cell-surface growth factor receptors become internalized through the process of receptor endocytosis, which plays an important role in the activation of signaling cascades from within the cell.[9,10] Indeed, it has been shown that endocytosis of the EGF receptor has to occur for the full activation of ERK.[11] Endocytosis is also critical in signal transduction through a G-protein-coupled receptor called PAR2, which upon activation is necessary for the subsequent activation and

Present address: A. Farooq, Department of Biochemistry & Molecular Biology, University of Miami School of Medicine, 1011 NW 15th Street, Miami, FL 33136, USA.

Abbreviations used: GST, glutathione-*S*-transferase; NOE, nuclear Overhauser effect; HSQC, heteronuclear single quantum coherence; CSI, chemical shift index.

E-mail addresses of the corresponding authors: ming-ming.zhou@mssm.edu; amjad@farooqlab.org

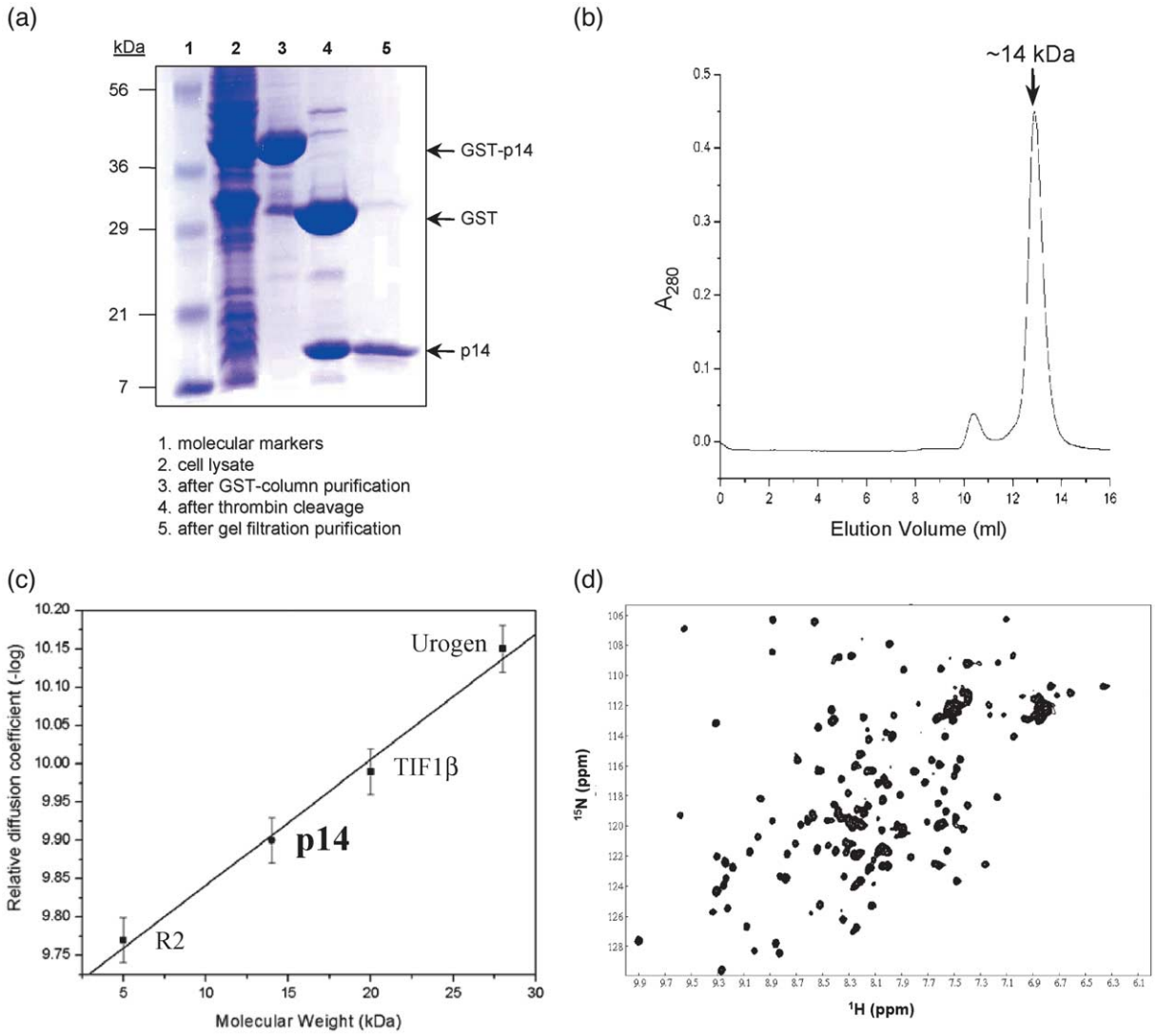

Figure 1 (*legend next page*)

endosomal localization of downstream effectors Raf and ERK.[12] It is now recognized that receptor endocytosis, which for a long time has been envisioned to be largely involved in down-regulation and recycling of cell surface receptors, provides another element of specificity by sequestering and localizing components in signaling pathways and, in so doing, serves as a site for the initiation of signaling from within the cell. In an attempt to identify proteins involved in the assembly of such signaling endosomes, Huber and coworkers used density gradient centrifugation to separate late endosomes from other organelles of the cell. Analysis of the peripheral proteins associated with the cytopalsmic face of late endosomes led to identification of a novel 14 kDa protein that they termed p14.[13] They further established that p14 specifically interacts with MP1, a scaffolding protein that brings ERK1 and its upstream activator MEK1 in close proximity and thereby potentiates signaling *via* the ERK signaling pathway.[14] More specifically, the interaction of p14 with MP1 recruits the latter to late endosomes and the endosomal localization of p14/MP1-MEK1-ERK1 scaffolding complex is required for signaling *via* ERK MAP kinase in an efficient and specific manner upon receptor stimulation.[15] Interestingly, this interaction appears transient, implying that p14/MP1 interaction may be the important determinant of not only spatial but also the temporal specificity of ERK signaling cascade.

In an effort to understand the molecular mechanisms underlying the recruitment of the MP1-MEK1-ERK1 signaling complex to late endosomes, we have determined the three-dimensional solution structure of the adaptor protein p14. The structure reveals a profilin-like fold with a central five-stranded β-sheet sandwiched between α-helices. Unlike profilin, however, p14 exhibits weak affinity for selective phosphoinositides but no affinity towards proline-rich sequences. Structural comparison between profilin and p14 reveals

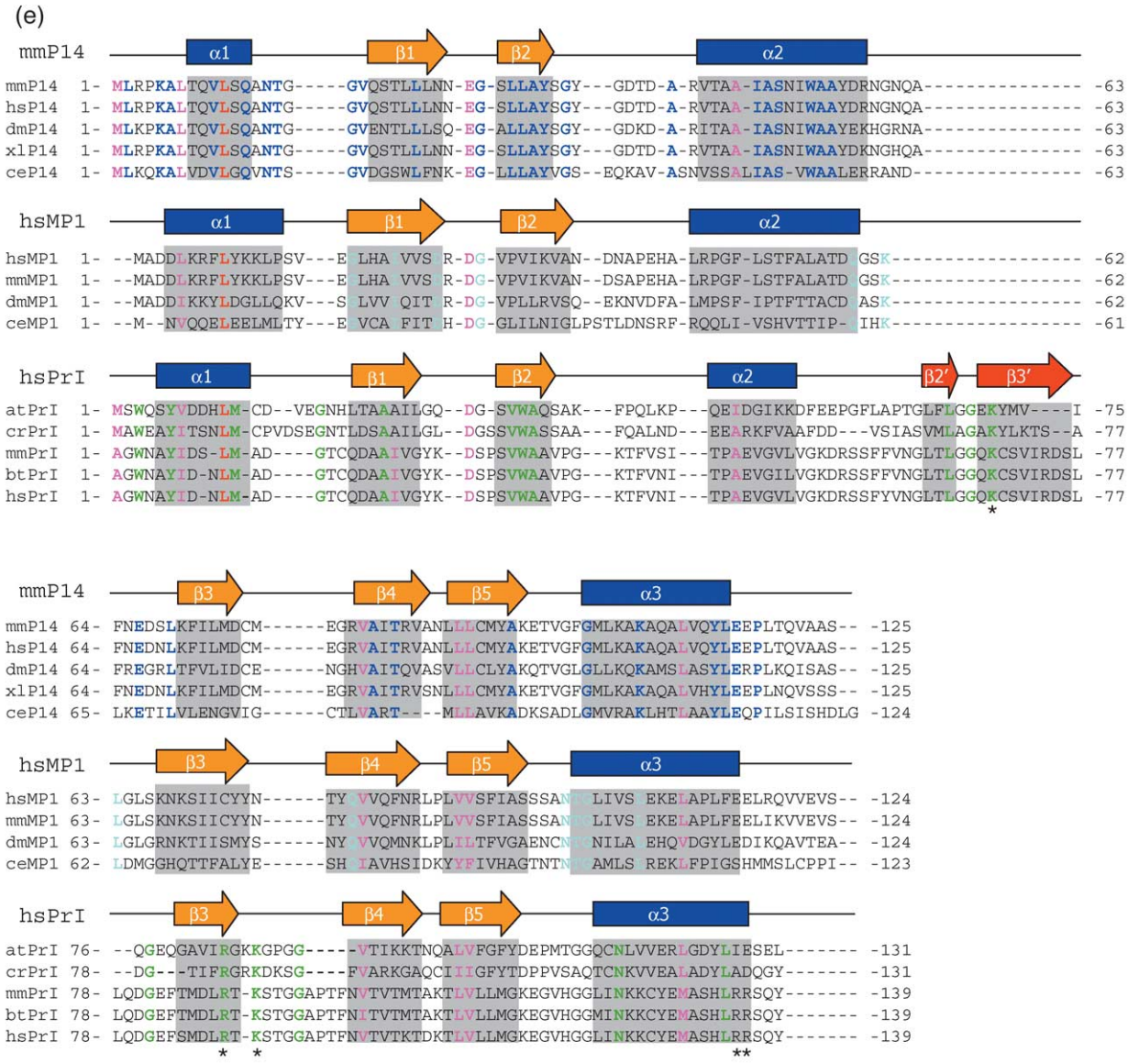

Figure 1. Preparation of the recombinant p14. (a) SDS-PAGE analysis showing purification of p14 from a bacterial expression system. (b) Gel filtration chromatograph of p14, showing that the protein exists as a monomer in solution. (c) Plot of relative diffusion coefficients as a function of molecular mass from p14 and the other three reference proteins (R2, ~5 kDa; TIF1β, ~20 kDa; Urogen, ~28 kDa). (d) 2D ^{1}H-^{15}N HSQC spectrum of p14 recorded at pH 6.5 and 298 K. (e) Sequence alignment of p14 (P14) from *Homo sapiens* (Q9Y2Q5), *Mus musculus* (Q9JHS3), *Drosophila melanogaster* (Q9V8I2), *Xenopus laevis* (Q7ZXB7) and *Caenorhabditis elegans* (Q9N2U6), MP1 from *H. sapiens* (068805), *M. musculus* (064304), *D. melanogaster* (609843) and *C. elegans* (741627), and profilin I (PrI) from *H. sapiens* (P07737), *M. musculus* (P10924), *Bos taurus* (P02584), *Arabidopsis thaliana* (Q42449) and *Chlamydomonas reinhardtii* (Q94KS3). The accession numbers given in parentheses were obtained from the SwissProt databank. Residues absolutely conserved in p14, MP1 and profilin I are shown in red while residues shown in purple are highly similar across three sets of proteins. Residues absolutely conserved in p14 alone are shown in blue, MP1 in cyan, and profilin I in green. Residues within profilins that bind phosphatidylinositol-4,5-bisphosphate (PI(4,5)P2) are indicated by asterisks. Regions of secondary structure elements in mouse p14, human MP1 and human profilin I are aligned on top of each group of sequences.

that the latter lacks signature residues required for strong interaction with these ligands. The interaction of p14 and MP1 was characterized by NMR and MP1 binding sites on p14 were mapped by chemical shift perturbation analysis of ^{15}N-labeled p14 that was titrated with an unlabeled MP1. We discuss the implications of these important findings on the possible biochemical function of p14.

Results and Discussion

Structure determination

The adaptor protein p14 was expressed as a full-length (residues 1–125), glutathione-*S*-transferase (GST)-fusion protein in a bacterial expression system and purified to apparent homogeneity as

judged by SDS-PAGE analysis (Figure 1(a)). The protein elutes with an apparent molecular mass of ~14 kDa in gel filtration chromatography (Figure 1(b)). Because a previous report suggested that p14 could weakly self-associate *in vitro*,[13] we further employed NMR self-diffusion measurements to assess the diffusion coefficient of p14, together with three other reference proteins. We found that the diffusion coefficient of p14 remained constant at ~14.5 kDa over a protein concentration range of 0.1–0.5 mM (Figure 1(c)). Taken together, these two independent lines of evidence strongly suggested that p14 exists as a monomeric form in solution. This conclusion is consistent with the excellent linewidth and good chemical shift dispersion of the backbone amide resonances of p14 as a protein of ~14 kDa, as shown in its 2D ^{1}H–^{15}N heteronuclear single quantum coherence (HSQC) spectrum (Figure 1(d)).

Various isotopically (^{2}H, ^{13}C and ^{15}N) labeled protein samples were purified using procedures as described in Experimental Procedures. The three-dimensional structure of p14 was determined using heteronuclear nuclear magnetic resonance (NMR) spectroscopy. The backbone and side-chain resonances of the protein were assigned from standard triple-resonance NMR experiments.[16] Secondary structure elements were identified from a combination of chemical shift index (CSI) analysis and a pattern of nuclear Overhauser effects (NOEs) characteristic of α-helices and β-strands. Figure 1(e) shows regions of secondary structure elements aligned on top of protein sequence. Cross-strand NOEs were used to align the various β-strands relative to each other in a central five-stranded antiparallel β-sheet sandwiched between α-helices. The 3D structure of the protein was determined from a total of 1556 NMR-derived distance, hydrogen bonding and torsional angle restraints (Table 1). A majority of distance restraints were manually assigned although ARIA[17] was also used in the later stages of the calculation. ARIA-assigned NOEs were manually checked and confirmed.

To provide an assessment of the convergence of the structure, superimposition of the core region of a family of 20 energy-minimized structures derived from the NMR restraints is depicted in Figure 2(a). All structures exhibit good geometry, with no violations of distance restraints greater than 0.5 Å and no dihedral angle violations larger than 5° (Table 1). The atomic root-mean-square deviations about the mean coordinate position of the backbone and side-chain atoms for the secondary structure elements are 0.48(±0.07) Å and 0.97(±0.11) Å, respectively. Detailed statistics for the structure of p14 are provided in Table 1. Except for the N and C-terminal residues 1–7 and 115–125, the overall structures are well defined.

p14 is constructed on a profilin-like fold

The structure of p14 is comprised of a central five-stranded (β1–β5) antiparallel β-sheet, arranged in the order 2-1-5-4-3, sandwiched between N and

Table 1. NMR statistics for the three-dimensional structure of p14

Total experimental restraints	1556	
Total NOE distance restraints	1340	
Ambiguous	68	
Unambiguous	1272	
Manually assigned	1071	
ARIA assigned	201	
Intra-residue	673	
Inter-residue	599	
Sequential $\|I-j\|=1$	227	
Medium $2\leq\|\iota-j\|\leq4$	134	
Long range $\|i-j\|>4$	238	
Hydrogen bond restraints	90	
Dihedral angle restraints	126	
Final energies (kcal/mol)[a]		
E_{TOT}	309.7±12.3	
E_{NOE}	58.7±10.6	
E_{DIH}	6.3±2.2	
E_{LJ}[b]	−461.3±16.4	
Ramachandron plot (%)[a]	Full molecule[c]	Secondary structure[d]
Most favorable region	70.1±2.4	94.8±1.7
Additionally allowed region	24.0±2.7	5.2±1.7
Generously allowed region	4.6±1.9	0.0±0.0
Disallowed region	1.3±1.1	0.0±0.0
Cartesian co-ordinate RMSDs (Å)[a,e]		
Backbone	0.79±0.10	0.48±0.07
Side-chain	1.30±0.13	0.97±0.11

[a] Based upon 20 lowest energy-minimized structures.
[b] The Lennard–Jones potential was not used during any refinement stage.
[c] Residues 8–114.
[d] Residues 9–13, 21–26, 30–34, 45–59, 70–75, 80–86, 89–95, 103–113.
[e] None of these final structures exhibit NOE-derived distance restraint violations greater than 0.5 Å or dihedral angle restraint violations greater than 5°.

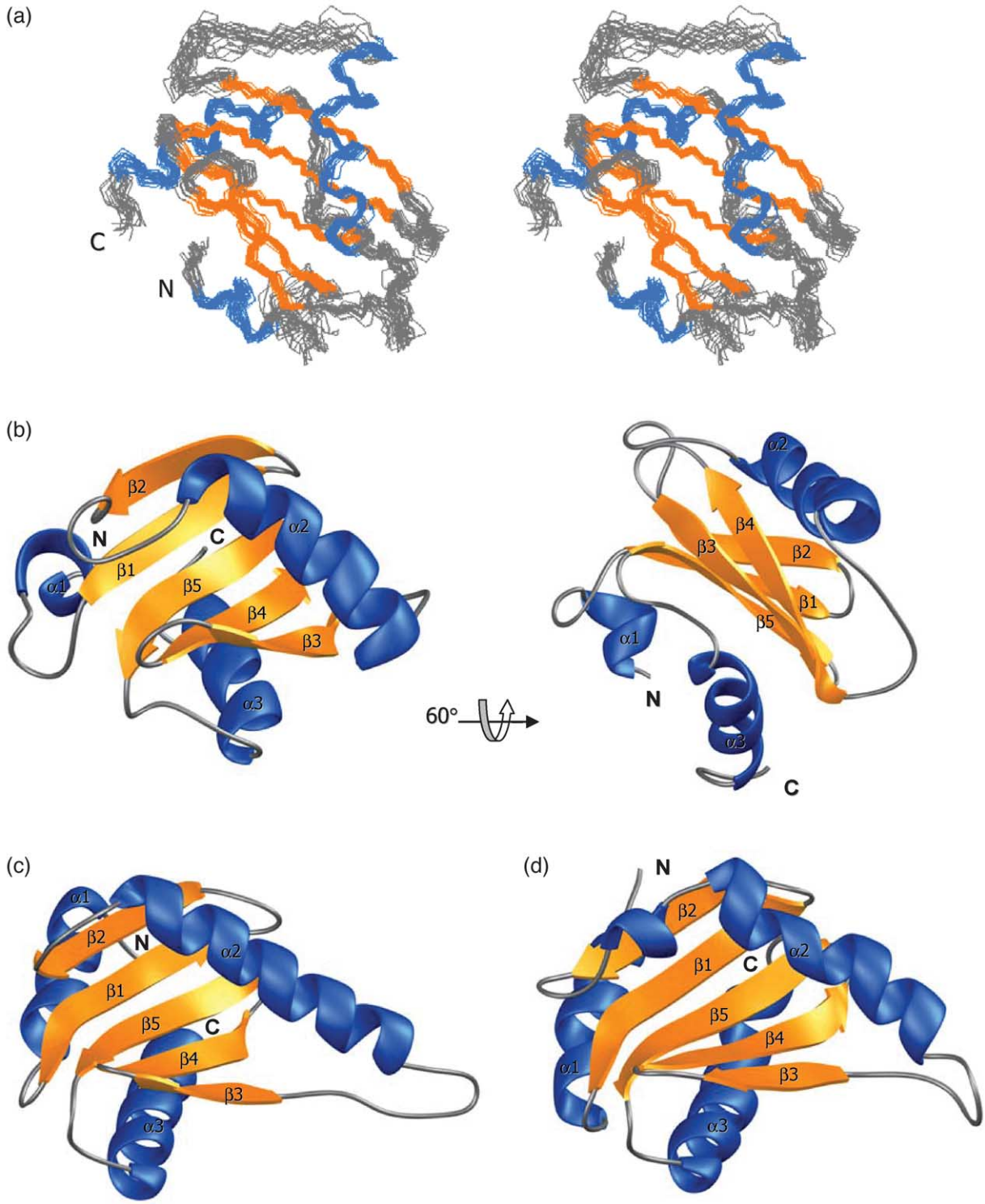

Figure 2. The three-dimensional structure of p14. (a) A stereoview showing superposition of a family of 20 energy-minimized NMR structures (residues 7–118). For clarity, the other N and C-terminal non-structured residues are omitted. (b) Ribbon diagrams of a representative structure from (a) in two alternative orientations related by a 60° rotation about the horizontal axis. Secondary structure regions defined by helices and strands are colored blue and yellow, respectively. The loop regions are shown in gray. (c) Ribbon diagram of p14 crystal structure obtained from MP1–p14 complex. (d) Ribbon diagram of MP1 crystal structure obtained from MP1–p14 complex.

C-terminal helices (α1 and α3) on one face of the molecule while a central helix (α2) lies on the opposite face (Figure 2(b)). During the preparation of our manuscript, the crystal structure of p14 in complex with MP1 appeared in the literature.[18,19] The structures of p14 in the free and the complex forms are very similar with some subtle differences (Figure 2(b) and (c)). For example, the N and

Table 2. A family of proteins with a profilin-like fold

Protein[a]	Topology	Function	PDB
Profilin	α1,α3[β2′↓-β3′↑-β3↓-β4↑-β5↓-β1↑-β2↓]α2	Actin polymerization	2PRF, 3NUL, 1PNE
p14	α1,α3[β3↓-β4↑-β5↓-β1↑-β2↓]α2	Receptor endocytosis	1SKO, 1SZV
Mglb	α1,α3[β3↓-β4↑-β5↓-β1↑-β2↓]α2	Unknown function	1J3W
Sedlin	α3-α4[β3↓-β4↑-β5↓-β1↑-β2↓]α2	Golgi transport	1H3Q
AP2 (μ2 ND)	α3-α4-α5-α6[β3↓-β4↑-β5↓-β1↑-β2↓]α2	Clathrin-mediated endocytosis	1GW5
AP2 (σ2)	α3-α4-α5-α6[β3↓-β4↑-β5↓-β1↑-β2↓]α2	Clathrin-mediated endocytosis	1GW5
GAF domain	α1′-α1,α3[β3↓-β4↑-β5↓-β1↑-β2↓]α2	cGMP receptor	1F5M, 1MC0
Srx domain	α3-α4-α5[β3↓-β4↑-β5↓-β1↑-β2↓]α2	Component of α-subunit of SRP	1NRJ
Ykt6 (ND)	α3-α4[β3↓-β4↑-β5↓-β1↑-β2↓]α2	Membrane trafficking	1H8M
PYP	α1′-α1[β3↓-β4↑-β5↓-β1↑-β2↓]α2′,α2	Phototactic response	3PYP
Dcus	α1′-α1″-α1,α3[β3↓-β4↑-β5↓-β1↑-β2↓]α2′,α2	Fumarate sensor	1OJG

[a] Abbreviations: ND, N-terminal domain; SRP, signal recognition particle; PYP, photoactive yellow protein.

C-terminal helices (α1 and α3) are both one turn shorter in the free structure than the MP1-complexed structure. This may contribute to the difference in relative orientation of the two helices: it is ~30° in the complex structure and ~45° in the free structure. Moreover, the helix α2 that is four turns and runs diagonally across one face of the central β-sheet is also one turn shorter in the free structure. This and a longer β3 strand in the free structure than in the MP1-bound structure may result in difference in the orientation of the loop that connects α2 and β3. Notably, these structural differences seen between the free and the complex forms of p14 match well with the main structural variations of the C-terminal α3 and the loop α2/β3 that were observed between different crystal forms of the p14/MP1 complex.[18] Thus, these results strongly suggest that the likely reason for such structural differences between the free and the complex forms of p14 is attributable to structural changes in p14 upon binding MP1.

Notably, despite low sequence similarity (Figure 1(e)), p14 and MP1 share a nearly identical structure as shown by the recently reported crystal structures of the complex[18,19] (Figure 2(c) and (d)). The two proteins form a heterodimer in a structurally symmetric manner with amino acid residues in α2 and β3 in p14 and MP1 at the dimer interface (Figure 5(c)). The corresponding amino acid residues in α2 and β3 from p14 and MP1 that are engaged in the dimer interface are not all conserved, and their flanking residues are highly variable (Figure 1(e)). As such, homo-dimerization of p14 or MP1 is less likely, which is consistent with our experimental observation that p14 exists predominantly in a monomeric state when free in solution (Figure 1(b) and (c)).

We performed structural homology search using DALI[20,21] and found a small group of proteins with similar structural folds to p14 (Table 2). Particularly, the p14 fold resembles that of profilins (Figure 3(a) and (b)), which are found in organisms ranging from plants to humans,[22–24] although profilins contain an insert of an additional antiparallel β-sheet formed by strands β2′ and β3′ between helix α2 and the strand β3 (Figure 1(c)). This comparison suggests that p14 is structurally related to profilins in evolution and that there could be some similarities between the function of p14 and profilins.

Profilins are a family of proteins that specifically interact with actin and regulate its polymerization in response to extracellular signals.[25] Actin polymerization is responsible for the organization of the microfilament system in eukaryotic cells and thus determines cell shape and motility. In addition to binding actin, profilins also bind phosphatidylinositol-4,5-bisphosphate (PtdIns(4,5)P2) and proline-rich sequences and thus play a critical role in signaling pathways.[26,27] The binding of profilins to PtdIns(4,5)P2 leads to dissociation of actin and subsequent membrane recruitment of profilins.

p14 interacts with selective phospholipids

Phosphoinositides (PIPs) present a mechanism for the recruitment of a diverse array of cellular proteins and modules to the membrane.[28] Given the structural similarity of p14 to profilins, we tested to see whether p14 may employ a similar mechanism for its attachment to the cytoplasmic face of late endosomes. As demonstrated in the protein-lipid overlay assay,[29] p14 showed weak binding to phosphatidylinositol-3-phosphate (PI(3)P) and phosphatidylinositol-4-phosphate (PI(4)P), but exhibited almost no affinity towards phosphatidylinositol-5-phosphate (PI(5)P), phosphatidylinositol-4,5-bisphosphate (PI(4,5)P2) or phosphatidylinositol-3,4,5-trisphosphate (PI(3,4,5)P3) (Figure 3(c)). Notably, the relatively weak interaction between p14 and PI(3)P or PI(4)P was sensitive to pH; the binding was best between pH 6–6.5 and much weaker or no binding at higher or lower pH. Based on quantification of p14 bound to PI(3)P or PI(4)P in a concentration manner, we estimated a dissociation constant of the binding to be 5–10 μM for both PI(3)P and PI(4)P. Taken together, these results imply that while p14 may be capable of interacting with selective phosphoinositides, the binding is likely of low affinity and highly dynamic, which is also seen with other known phosphoinositide binding protein modules such as pleckstrin homology (PH), FYVE and FERM domains.[28]

In an attempt to understand such functional differences at the molecular level, we performed a

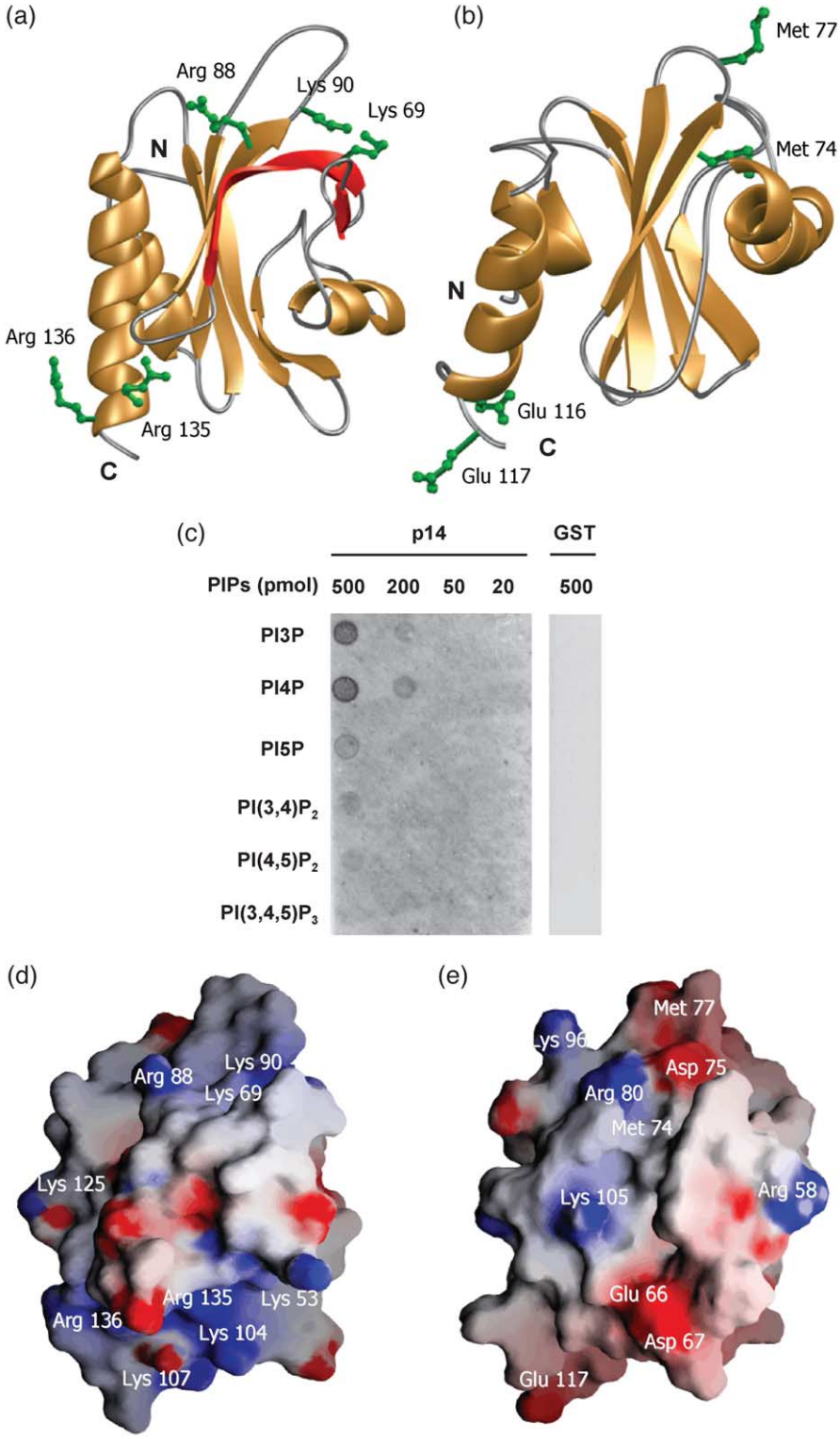

Figure 3. Binding to phosphoinositides. (a) Ribbon diagram of human profilin I (residues 3–138) showing side-chains of residues involved in binding phosphatidylinositol-4,5-bisphosphate at two distinct sites constituted by residues Arg88, Lys90 and Lys69, and Arg135 and Arg136. An insert of antiparallel β-sheet formed by strands β2′ and β3′ in profilin I is shown in red. (b) Ribbon diagram of mouse p14 (residues 7–118) showing side-chains of equivalent residues at positions corresponding to residues shown in profilin I above. (c) GST-fusion p14 binding to phosphoinositides, as assessed by a protein-phospholipid overlay assay. The phospholipid-bound p14 signal is visualized by Western blots using anti-GST antibodies. (d) Corresponding surface potential views of profilin I and p14, respectively. Residues in profilin I involved in binding PI(4,5)P2 and equivalent residues in mouse p14 are labeled. Additional acidic and basic residues are also shown.

structure-based sequence alignment of p14 and profilin, which share little sequence similarity (Figure 1(e)). It has been reported that human profilin contains two distinct PI(4,5)P2 binding sites.[27] One site is formed by residues Arg88, Lys90 and Lys69 located, respectively, in the strands β3′ and β3 and the loop β3-β4, while the second site is constituted by residues Arg135 and Arg136 located at the C terminus of the C-terminal helix α3 (Figure 3(a)). Indeed, mouse and bovine profilins, in which these residues are conserved, show high binding affinity towards PI(4,5)P2, while profilins from plant and green algae, in which Arg135 and Arg136 are replaced by hydrophobic or acidic residues, exhibit significantly diminished affinity towards PI(4,5)P2 or other PIPs.[24] In contrast, none of these residues are conserved in p14. Moreover, the strand β3′ that contains Lys69 is completely absent in p14, while Arg88, Arg90, Arg135 and Arg136 are replaced by Met77, Met74, Glu116 and Glu117, respectively, in both human and mouse p14 (Figure 3(b)). Mapping of protein electrostatic potential onto molecular surface shows that the two well-defined positive pockets for binding PIP2 in human profilin are absent from mouse p14 (Figure 3(d) and (e)). Instead, p14 contains Arg80, and Lys96 and Lys105 that are not clustered but rather localized in proximity on one side of the protein surface (Figure 3(e)). Therefore, the lack of positively charged residues clustered at these regions may account for the weak interactions of p14 with PI(3)P and PI(4)P.

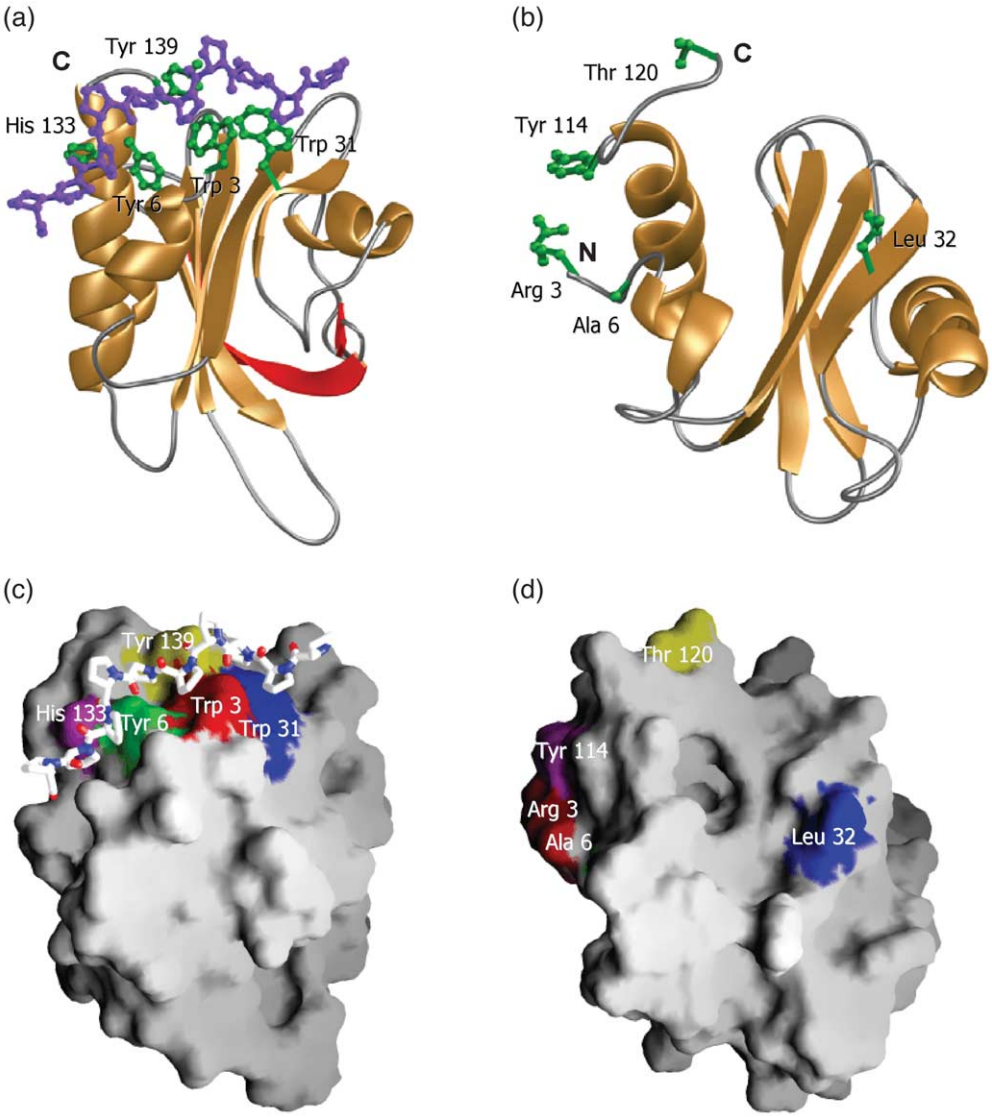

Figure 4. p14 exhibits no affinity towards proline-rich sequences. (a) Ribbon diagram of human profilin I (residues 3–139) in complex with a poly-L-proline decameric peptide (purple). An insert of antiparallel β-sheet formed by strands β2′ and β3′ in profilin I is shown in red. (b) Ribbon diagram of mouse p14 (residues 3–120) showing side-chains of residues at positions corresponding to those in profilin I. (c) and (d) Corresponding surface views of profilin I and p14, respectively. Residues in profilin I involved in poly-L-proline peptide binding and corresponding residues in mouse p14 are color-coded.

Proline-rich sequences are not targets for p14

p14 recruits the MP1-MEK1-ERK1 signaling complex to late endosomes through its interaction with MP1 and/or MEK1, the upstream kinase activator of ERK1.[13] Notably, MEK1 contains a proline-rich sequence (PRS), residues 281–308, that has been suggested to be important for p14-MP1-MEK-ERK1 complex formation. In light of the new structural knowledge of p14, which contains the same structural fold profilins that are known to bind specifically proline-rich sequences, we postulated whether the PRS motif might serve as a potential docking site for p14. To test the possibility that p14 binds proline-rich sequences in a biologically relevant context, we titrated the protein against a 28-residue peptide (DAAETPPRPRTPGRPLSSYGMDSRPPMA) derived from the PRS in MEK1. As monitored in the 2D ^{1}H–^{15}N HSQC spectra, the backbone amide signals of the protein exhibited almost no any significant chemical shift perturbation upon addition of the MEK1 PRS peptide up to 1 : 10 molar ratio of protein to peptide (0.3 mM *versus* 3 mM; data not shown), suggesting that p14 most likely does not bind this proline-rich sequence peptide in solution.

While there are several families of proteins and protein modules that have been discovered to be able to bind proline-rich sequences,[30,31] one thing that they all have in common is their ability to employ a conserved patch of aromatic residues to bind proline-rich sequences. Structure comparison of p14 with human profilin illustrates this mode of molecular recognition clearly.[26] Figure 4(a) shows a Ribbons representation of profilin bound to a ten-residue poly-L-proline (PLP) sequence.[26] The residues that are directly involved in PLP binding are Trp3, Tyr6, Trp31, His133 and Tyr139. These residues are absolutely conserved in mouse and bovine profilins, implying their conserved role in binding PLP sequences. However, the corresponding residues in p14, on the basis of structure-based sequence alignment (Figure 1(c)), are Arg3, Ala6, Leu32, Tyr114 and Thr120 (Figure 4(b)). Out of the five aromatic residues involved in PLP binding in profilins, only one aromatic residue (Tyr114) is conserved in p14. Furthermore, the Ribbons representation shows that p14 not only lacks the aromatic residues for binding proline-rich sequences but that the corresponding residues do not constitute a closely knit binding pocket as observed in human profilin (Figure 4(a) and (b)). The surface views further indicate that a well-formed surface groove for binding PLP in human profilin is absent in p14 (Figure 4(c) and (d)).

Interaction of p14 with MP1

To identify MP1 interaction sites on p14 surface, we performed NMR titration of ^{15}N-labeled p14 with unlabeled MP1 by recording a series of 2D ^{1}H-^{15}N HSQC spectra of p14 as a function of MP1 concentration. The MP1 interaction induced chemical shift changes are color-coded on the surface of the p14 structure (Figure 5(a)). Amino acid residues of p14 that exhibit major chemical shift perturbations appear to be located in the p14/MP1 heterodimer interface (Figure 5(b)). As shown in the crystal structure of the complex, Asp67, Lys70 and Asp75 in p14 form hydrogen bonds and/or salt bridges with Thr77, Asn76 and Lys69 of MP1; Leu69 and Met74 of p14 have hydrophobic interactions with Ile71 and Tyr75 of MP1, respectively. The side-chain of Tyr56 of p14 forms a hydrogen bond with Gln83, and also interacts with Thr52 of MP1. Notably, residues of p14 that exhibit the most dramatic chemical shift changes are located in two sequences in α2-β3-β4-β5-α3 of the protein containing Glu66-Met77 and Lys80-Thr84. These most perturbed regions observed in NMR titration overlap very well with the p14/MP1 interface characterized by the crystal structure of the complex (Figure 5(b)). Taken together, our characterization of p14/MP1 interaction in solution by NMR further helps explain the structural differences of p14 between the free and MP1-bound states.

In conclusion, the adaptor protein p14 that is associated with the cytoplasmic face of late endosomes in receptor endocytosis recruits the MP1-MEK1-ERK1 signaling complex to the endosomal membrane through its specific interaction with the scaffolding protein MP1.[13–15] Unraveling the underlying molecular mechanisms involved in these interactions thus remains an important endeavor not only towards a better understanding of the process of receptor endocytosis but also to shed further light on the spatial and temporal specificity that is a hallmark of MAP kinase signaling cascades. Here, we have shown that p14 shares the same structural fold as that found in profilins. However, unlike profilins, p14 appears to interact weakly but selectively with PI(3)P and PI(4)P *in vitro*, but not with proline-rich sequences. These results suggest that p14 may be associated with the endosomal membranes through selective phosphoinositide binding and also possibly through electrostatic and hydrogen bonding interactions with specific endosomal integral membrane proteins. These are indeed the mechanisms by which a vast majority of peripheral membrane proteins attach to cell membranes. The availability of the new three-dimensional structure of p14 reported here will facilitate further elucidation of its molecular functions that play an important role in regulating MAP kinase-mediated receptor endocytosis.

Experimental Procedures

Sample preparation

Mouse p14 was cloned by amplifying p14 cDNA using polymerase chain reaction (PCR) from a total mouse brain cDNA library (Invitrogen) and sub-cloned into the bacterial expression vector pGEX-6P-1 (Pharmacia). This

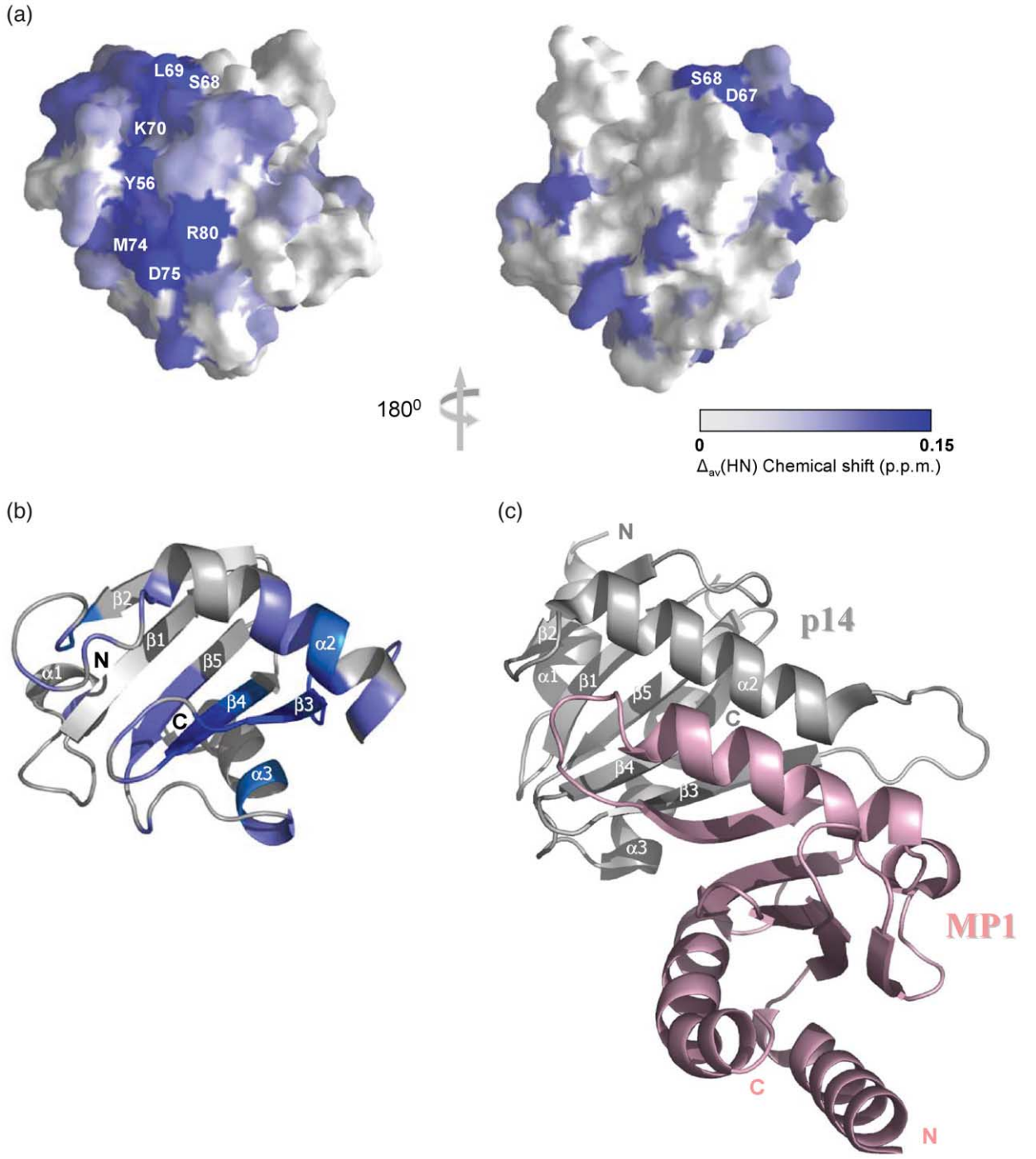

Figure 5. Mapping of MP1 interaction site on p14 by NMR. (a) Molecular surface view of p14 highlighting protein residues showed major chemical shift perturbations upon binding MP1. The residues are color-coded according to the extent of chemical shift changes from white to blue. (b) Ribbon diagram of the free p14 showing residues that exhibited major chemical shift changes. These residues are color-coded similarly as in (a), large chemical shift changes in blue (Tyr56, Asp67-Asp75, Lys80-Ala82), medium in marine (Tyr34, Ser35, Ala54, Aal55, Asn62, Glu66, Met77, Ile83, Thr84, Leu104 and Lys105), and small in gray. (c) Ribbon diagram of the crystal structure of the p14/MP1 complex.

vector, when transformed into *Escherichia coli* (strain BL21 DE3), expresses p14 as a GST-fusion protein with a PreScission protease cleavage site that was used to cleave the GST-tag from the fusion protein after purification. Recombinant p14 protein was purified as follows. Bacterial cells containing the p14 expression vector were grown in LB or minimal media at 25 °C. Protein expression was induced by the addition of 0.2 mM isopropyl-1-thio-β-D-galactopyranoside to the bacterial culture at a cell density of about 0.6 absorbance units measured at 600 nm. The bacterial culture was further grown for three hours at 25 °C. The cells were then spun down with Sorvall RC5C plus centrifuge and SS34 rotor and disrupted using a tip sonicator in 50 mM sodium phosphate, 200 mM NaCl, 5 mM β-mercaptoethanol (pH 8.0).

The GST-fusion protein was purified by using a glutathione-Sepharose column first, and then was passed through gel filtration chromatography to remove some high molecular mass impurity. The GST-tag was removed by the cleavage of the fusion protein with PreScission protease to generate p14 protein with the following additional residues GPLGS at the N terminus. The protein was then subjected to gel filtration chromatography to remove the GST-tag. The protein elutes with an apparent molecular mass of ~14 kDa, implying that p14 exists in a monomeric form under these conditions. Uniformly ^{15}N and $^{15}N/^{13}C$-labeled proteins were made by growing bacteria in a minimal medium containing $^{15}NH_4Cl$ with or without [$^{13}C_6$]glucose. A uniformly $^{15}N/^{13}C$-labeled and fractionally deuterated protein sample was prepared by using a medium containing 75% ^2H_2O.

The mouse MP1 gene was PCR amplified from mouse brain cDNA. The amplified MP1 fragment was inserted into the BamHI-Xho I sites of the modified plasmid pET-28a (Novagen). The modified pET-28a plasmid harboring the MP1 gene was then transformed into *E. coli* BL21 (DE3) host cells.

MP1 recombinant protein was purified as follows. Host cells containing the MP1 plasmid construct were grown in LB medium at 37 °C till the A_{600} reached about 1.0. MP1 expression was induced by the addition of IPTG to final concentration of 0.3 mM, and the culture temperature was decreased to 18 °C. Protein expression lasted for about eight hours. Recombinant MP1 was purified by a combination of a Ni^{2+}-NTA affinity column and other chromatographic techniques. Cell pellets were resuspended in 20–30 ml of Ni^{2+}-NTA column binding buffer (20 mM Tris–HCl (pH 7.9), 10 mM imidazole, 300 mM NaCl) containing 1 mM phenylmethylsulfonyl fluoride. Cells were disrupted by a French Press, and the lysate was centrifuged at 16,000 rpm for 30 minutes. Soluble MP1 in the supernatant was purified on the Ni^{2+}-NTA column following the instructions of the manufacturer (Novagen). The His tag was removed by adding thrombin to the MP1 eluted from the Ni^{2+}-NTA column, after the cleavage the protein was directly applied to a Superdex 75 gel filtration column (Amersham Pharmacia Biotech) to remove small amounts of contaminant proteins. MP1 was eluted with 50 mM Tris–HCl buffer at pH 7.5 containing 1 mM EDTA, 1 mM DTT. The fractions containing MP1 were combined and dialyzed overnight against 100 mM PO_4^{3-} buffer containing 1 mM DTT at pH 6.5 and stored at 4 °C.

NMR spectroscopy

NMR samples typically contained ~0.5 mM protein in 50 mM sodium phosphate, 100 mM NaCl and 5 mM DTT-d_{10} in $H_2O/^2H_2O$ (9/1) at pH 6.5. All NMR spectra were acquired at 25 °C on a 600 MHz or 500 MHz Bruker DRX NMR spectrometer. The backbone and side-chain ^1H, ^{13}C, and ^{15}N resonances of the protein were assigned using deuterium-decoupled triple resonance spectra of HNCA, HN(CO)CA, HNCACB, HN(CO)CACB, and (H)C(CO)NH-TOCSY recorded on a uniformly $^{15}N/^{13}C$-labeled and fractionally deuterated protein.[16] The side-chain assignments were completed with 3D HCCH-TOCSY[32] data collected from a uniformly $^{15}N/^{13}C$-labeled protein. NOE-derived distance restraints were obtained from ^{15}N or ^{13}C-edited 3D NOESY spectra. Backbone torsion angles ϕ and ψ were calculated from the chemical shift resonances of H^{α} and C^{α} backbone atoms referenced against the initial protein structure calculated in the absence of any torsion angle restraints using the semi-empirical program TALOS.[33] Slowly exchanging amide protons were identified from a series of 2D ^{15}N-HSQC spectra recorded after the H_2O buffer was changed to ^2H_2O buffer. All NMR spectra were processed with NMRPipe/NMRDraw[34] and analyzed by NMRView.[35]

Diffusion coefficient measurement

The simulated echo with longitudinal eddy current delay (STE-LED) method[36] was used to run diffusion ordered spectroscopy that measures translational self-diffusion coefficient of a protein on a 500 MHz NMR spectrometer. We applied the standard pulse sequence from Bruker with combined Watergate and presaturation sequence to measure the diffusion coefficients for p14 and three other reference proteins of different molecular mass (R2 of ~5 kDa, TIF1β of ~20 kDa and Urogen of ~28 kDa) at protein concentrations of 0.1 mM and 0.4 mM.

NMR titration of p14 with MP1

Titrations of ^{15}N-labeled p14 with unlabeled MP1 were performed by recording a series of 2D ^1H-^{15}N HSQC spectra of ^{15}N-p14 as a function of increasing MP1 concentration. The weighted average chemical shift differences,[37] $\Delta(HN)_{av}$, were calculated for the backbone amide ^1H and ^{15}N resonances, using the equation: $\Delta(HN)_{av} = \{((\Delta H)^2 + (\Delta N/5)^2)/2\}^{1/2}$, where ΔH and ΔN are chemical shift differences for ^1H and ^{15}N, respectively.

Structure calculations

p14 structure was calculated with a distance geometry—simulated annealing protocol using the X-PLOR program.[38] The initial structure calculations were performed using manually assigned NOE-derived distance restraints. The converged structures were then used for the iterative automated assignment of the NOE spectra by ARIA,[17] which integrates with X-PLOR for structure refinement. The NOE-derived restraints were categorized based on the observed NOE peak intensities. ARIA-assisted assignments were manually checked and confirmed. Hydrogen bond and angular restraints were added at a later stage in structure calculation.

Protein and phospholipid overlay assay

The p14 and phosphoinositide overlay assay was carried out using a similar procedure to that described.[29] Phosphoinositides (Cayman) were made as 1 M stock solution in methanol:chloroform (1 : 1, v/v). The stock solution was diluted to different concentrations with methanol:chloroform:water (2 : 1 : 0.8, by vol.), and dotted ~1 μl onto the C-Extra Nitrocellulose membrane (Amersham Bioscience) that was allowed to air dry for one hour. The membrane was washed with blocking buffer (50 mM Tris (pH 7.0), 150 mM NaCl, 0.1% Tween 20, 2 mg/ml BSA) at room temperature for one hour, and then incubated with GST-fusion p14 (~5 μM) at 4 °C overnight, followed by washing with a buffer containing 50 mM Tris (pH 7.0), 150 mM NaCl and 0.1% Tween 20 at room temperature. p14 bound to the phosphoinositides was visualized in Western blots by anti-GST antibody and horseradish-peroxidase-conjugated goat anti-rabbit IgG.

Protein Data Bank accession codes

The structure coordinates of p14 have been deposited in the RCSB Protein Data Bank under the ID code 1SZV.

Acknowledgements

This work was supported by a grant from the National Institute of Health to M.-M.Z. (CA80938).

References

1. Hunter, T. (2000). Signaling—2000 and Beyond. *Cell*, **100**, 113–127.
2. Forman-Kay, J. D. & Pawson, T. (1999). Diversity in protein recognition by PTB domains. *Curr. Opin. Struct. Biol.* **9**, 690–695.
3. Kavanaugh, W. M. & Williams, L. T. (1994). An alternative to SH2 domains for binding tyrosine-phosphorylated proteins. *Science*, **266**, 1862–1865.
4. Blaikie, P., Immanuel, D., Wu, J., Li, N., Yajnik, V. & Margolis, B. (1994). A region in Shc distinct from the SH2 domain can bind a tyrosine phosphorylated growth factor receptor. *J. Biol. Chem.* **269**, 32031–32034.
5. Pelicci, G., Lanfrancone, L., Grignani, F., McGlade, J., Cavallo, F., Forni, G. *et al*. (1992). A novel transforming protein (Shc) with an SH2 domain is implicated in mitogenic signal transduction. *Cell*, **70**, 93–104.
6. Obermeier, A., Lammers, R., Weismuller, K., Schlessinger, J. & Ullrich, A. (1993). Identification of Trk binding sites for Shc and phosphatidylinositol 3′-kinase and formation of a multimeric signaling complex. *J. Biol. Chem.* **268**, 22963–22966.
7. Cahill, M. A., Hanknecht, R. & Nordheim, A. (1996). Signalling pathways: jack of all cascades. *Curr. Biol.* **6**, 16–19.
8. Treisman, R. (1996). Regulation of transcription by MAP kinase cascades. *Curr. Opin. Cell Biol.* **8**, 205–215.
9. DiFore, P. P. & Gill, G. N. (1999). Endocytosis and mitogenic signaling. *Curr. Opin. Cell Biol.* **11**, 483–488.
10. Lemmon, S. K. & Traub, L. M. (2000). Sorting in the endosomal system in yeast and animal cells. *Curr. Opin. Cell Biol.* **12**, 457–466.
11. Kranenburg, O., Verlaan, I. & Moolenaar, W. H. (1999). Dynamin is required for the activation of MAP kinase by MAP kinase kinase. *J. Biol. Chem.* **274**, 35301–35304.
12. DeFea, K. A., Zalevsky, J., Thoma, M. S., Dery, O., Mullins, R. D. & Bunnett, N. W. (2000). Beta-arrestin-dependent endocytosis of PAR2 is required for intracellular targeting of activated ERk1/2. *J. Cell Biol.* **148**, 1267–1281.
13. Wunderlich, W., Fialka, I., Teis, D., Alpi, A., Pfeifer, A., Parton, R. G. *et al*. (2001). A novel 14-kilodalton protein interacts with the mitogen-activated protein kinase scaffold mp1 on a late endosomal/lysosomal compartment. *J. Cell Biol.* **152**, 765–776.
14. Schaeffer, H. J., Catling, A. D., Eblen, S. T., Collier, L. S., Krauss, A. & Weber, M. J. (1998). MP1: a MEK binding partner that enhances enzymatic activation of the MAP kinase cascade. *Science*, **281**, 1668–1671.
15. Teis, D., Wunderlich, W. & Huber, L. A. (2002). Localization of the MP1-MAPK scaffold complex to endosomes is mediated by p14 and required for signal transduction. *Dev. Cell*, **3**, 803–814.
16. Yamazaki, T., Lee, W., Arrowsmith, C. H., Mahandiram, D. R. & Kay, L. E. (1994). A suite of triple resonance NMR experiments for the backbone assignment of 15N, 13C, 2H labeled proteins with high sensitivity. *J. Am. Chem. Soc.* **116**, 11655–11666.
17. Nilges, M. & O'Donoghue, S. (1998). Ambiguous NOEs and automated NOE assignment. *Prog. NMR Spectroscopy*, **32**, 107–139.
18. Kurzbauer, R., Teis, D., de Araujo, M. E., Maurer-Stroh, S., Eisenhaber, F., Bourenkov, G. P. *et al*. (2004). Crystal structure of the p14/MP1 scaffolding complex: how a twin couple attaches mitogen-activated protein kinase signaling to late endosomes. *Proc. Natl Acad. Sci. USA*, **101**, 10984–10989.
19. Lunin, V. V., Munger, C., Wagner, J., Ye, Z., Cygler, M. & Sacher, M. (2004). The structure of the MAPK scaffold, MP1, bound to its partner, p14. A complex with a critical role in endosomal map kinase signaling. *J. Biol. Chem.* **279**, 23422–23430.
20. Holm, L. & Sander, C. (1995). Dali: a network tool for protein structure comparison. *Trends Biochem. Sci.* **20**, 478–480.
21. Lo Conte, L., Ailey, B., Hubbard, T. J., Brenner, S. E., Murzin, A. G. & Chothia, C. (2000). SCOP: a structural classification of proteins database. *Nucl. Acids Res.* **28**, 257–259.
22. Schutt, S. E., Myslik, J. C., Rozycki, M. D., Goonesekere, N. C. W. & Lindberg, U. (1993). The structure of crystalline profilin-actin. *Nature*, **365**, 810–816.
23. Vinson, V. K., Archer, S. J., Lattman, E. E., Pollard, T. D. & Torchia, D. A. (1993). Three-dimensional solution structure of Acanthamoeba profilin I. *J. Cell Biol.* **122**, 1277–1283.
24. Orengo, C. A., Michie, A. D., Jones, S., Jones, D. T., Swindells, M. B. & Thornton, J. M. (1997). CATH—A hierarchic classification of protein domain structures. *Structure*, **5**, 1093–1108.
25. Machesky, L. M. & Pollard, T. D. (1993). Profilin as a potential mediator of membrane cytoskeleton communication. *Trends Cell Biol.* **3**, 381–385.
26. Mahoney, N. M., Rozwarski, D. A., Fedorov, E., Fedorov, A. A. & Almo, S. C. (1999). Profilin binds proline-rich ligands in two distinct amide backbone orientations. *Nature Struct. Biol.* **6**, 666–671.
27. Skare, P. & Karlsson, R. (2002). Evidence for two interaction regions for phosphatidyl-4,5-bisphosphate on mammalian profilin I. *FEBS Letters*, **522**, 119–124.
28. Cullen, P. J., Cozier, G. E., Banting, G. & Mellor, H. (2001). Modular phosphoinositide-binding domains—their role in signalling and membrane trafficking. *Curr. Biol.* **11**, R882–R893.
29. Dowler, S., Kular, G. & Alessi, D. R. (2002). Protein lipid overlay assay. *Sci. STKE*, **129**, 16.
30. Huang, X., Poy, F., Zhang, R., Joachimiak, A., Sudol, M. & Eck, M. J. (2000). Structure of a WW domain containing fragment of dystrophin in complex with beta-dystroglycan. *Nature Struct. Biol.* **7**, 634–638.
31. Bedford, M. T., Chan, D. C. & Leder, P. (1997). FBP WW domains and the Abl SH3 domain bind to a specific class of proline-rich ligands. *EMBO J.* **16**, 2376–2383.
32. Logan, T. M., Olejniczak, E. T., Xu, R. X. & Fesik, S. W. (1993). A general method for assigning NMR spectra of denatured proteins using a 3D HC(CO)NH-TOCSY triple resonance experiments. *J. Biolmol. NMR*, **3**, 225–231.
33. Cornilescu, G., Delaglio, F. & Bax, A. (1999). Protein

backbone angle restraints from searching a database for chemical shift and sequence homology. *J. Biomol. NMR*, **13**, 289–302.
34. Delaglio, F., Grzesiek, S., Vuister, G. W., Zhu, G., Pfeifer, J. & Bax, A. (1995). NMRPipe: a multidimensional spectral processing system based on UNIX pipes. *J. Biomol. NMR*, **6**, 277–293.
35. Johnson, B. A. & Blevins, R. A. (1994). NMRView: a computer program for the visualization and analysis of NMR data. *J. Biomol. NMR*, **4**, 603–614.
36. Altieri, A. S., Hinton, D. P. & Byrd, R. A. (1995). Association of biomolecular systems *via* pulsed field gradient NMR self-diffusion measurements. *J. Am. Chem. Soc.* **117**, 7566–7567.
37. Grzesiek, S., Bax, A., Clore, G. M., Gronenborn, A. M., Hu, J. S., Kaufman, J. *et al*. (1996). The solution structure of HIV-1 Nef reveals an unexpected fold and permits delineation of the binding surface for the SH3 domain of Hck tyrosine protein kinase. *Nature Struct. Biol.* **3**, 340–345.
38. Brunger, A. T. (1993). X-PLOR *Version 3.1: a system for X-ray crystallography and NMR*. Version 3.1 edit., Yale University Press, New Haven, CT.

Edited by P. Wright

(Received 8 September 2004; received in revised form 28 December 2004; accepted 12 January 2005)